PERGAMON

International Journal of Multiphase Flow 25 (1999) 433–457

International Journal of Multiphase Flow

Flow regime identification in microgravity two-phase flows using void fraction signals

D.C. Lowe *, K.S. Rezkallah

Department of Mechanical Engineering, University of Saskatchewan, Saskatoon, Canada, S7N 5A9

Received 26 November 1997; received in revised form 30 August 1998

Abstract

A concave parallel plate capacitance sensor has been developed to measure the two-phase flow void fraction for the purpose of objectively identifying flow regimes. The sensor has been used in conjunction with a two-phase flow loop onboard the NASA Lewis DC-9 microgravity aircraft, and data was recently collected. The void fraction time trace and probability density function, along with high speed video images of the flow were used to determine a more objective method of flow regime identification than what is possible through examination of video images alone. A set of criteria was developed to allow the identification of the flow regimes and their transitions through the examination of the void fraction probability density function. Against these criteria, flow regime transition models in the literature for microgravity gas–liquid two-phase flows were evaluated.

Keywords: Microgravity; Two-phase; Flow regime identification

1. Introduction

Two-phase flow is becoming increasingly important in many processes and power-generation technologies as well as in evolving future space missions. Examples of the latter are mining extra-terrestrial soils, physical and chemical processes in spacecraft systems, life support systems, bio-fluids and cryogenics, and use of in-situ resources and power generation in extra-terrestrial environments.

There are several reasons for investigating two-phase flow under microgravity conditions. First, it provides data on the aforementioned processes for the design and testing of space-

* Corresponding author.

0301-9322/99/$ - see front matter
PII: S0301-9322(98)00058-5

based hardware. It also lends to a better understanding of two-phase gas–liquid flows. The virtual absence of gravity permits investigation into how minor forces such as surface tension could affect the flow in the absence of the more dominant forces on earth due to gravitational acceleration.

It has been previously shown (Zhao and Rezkallah, 1993) that under microgravity conditions four flow regimes exist. As illustrated by Fig. 1, these are: bubbly flow, characterized by discrete gas bubbles flowing in the liquid; slug flow, consisting of Taylor bubbles having rounded nose and tail and separated by liquid slugs which may or may not contain smaller gas bubbles; transitional flow, characterized by the liquid flowing as a film at the tube wall and the gas phase flowing in the center with the frequent appearance of chaotic, frothy liquid slugs; and annular flow in which the liquid flows as a film along the tube wall and the gas flows uninterrupted through the center. While these four flow regimes can be used to describe two-phase flow in both small and large diameter tubes, the boundaries between them are not constant and may vary with tube diameter and other flow variables (Bousman et al., 1996). Since many two-phase flow models are flow regime dependent, a method that can accurately and objectively determine the flow regimes is highly desirable.

One of the shortcomings of two-phase flow analysis is the fact that, in most cases, the flow regimes are determined subjectively. Flow and/or flow transition identification are often made using recorded flow images, a process that is very time consuming and subjective in nature. This may account for large discrepancies between reported data. However, many researchers have shown that under normal gravity conditions, void fraction can be used to add some objectivity to the flow regime identification. In general, such methods involve the use of the probability density function (PDF) of the void fraction signals. One of the earliest studies using

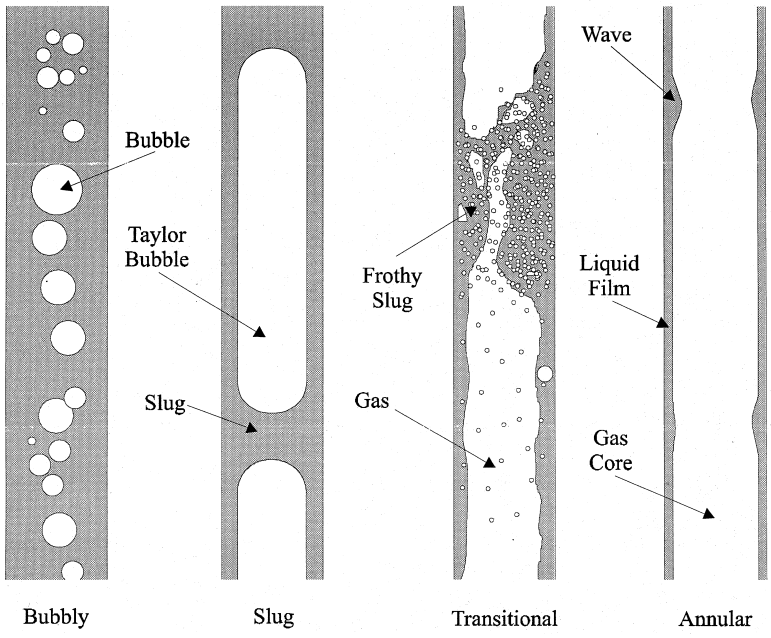

Fig. 1. Sketch of microgravity two-phase flow regimes.

this method was conducted by Jones and Zuber (1975), while some of the more recent efforts have been reported by Song et al. (1995) and Costigan and Whalley (1997).

Jones and Zuber (1975) investigated two-phase air–water flow in a vertical square channel 4.98 mm deep by 63.50 mm wide. Void fraction was measured using an X-ray system. Flow regime identification was achieved by plotting probability density functions (PDF) of each flow setting. Their results showed that slug flow was characterized by a double peak in the PDF plot, while bubble and annular flows had only a single peak at low and high void fractions, respectively. Their study served as a basis for much of the work done in recent years.

More recently Song et al. (1995) investigated air–water flow in a 25 mm inside diameter vertical tube. Void fraction was measured using an impedance sensor, and the data was used to determine several statistical parameters. These included the signal to noise ratio (SNR), power spectral density functions (PSDF), autocorrelation functions (ACF), and the PDF. Through visual observations and examination of the PDF, SNR, and the time traces of the void signals, they were able to characterize bubble and slug flows. Song et al. (1995) found that strong indicators of the bubble-to-slug transition are the shape of the PDF, a sharp increase in the SNR when the gas flow is increased, and the distinct change in apparent time scales calculated from the ACF. These apparent time scales are defined as the time required for the ACF, calculated either from the instantaneous signal or from the fluctuating portion of the signal, to reach half its maximum.

Costigan and Whalley (1997) investigated vertical air–water flow in a 32 mm inner diameter tube. In that study, void fraction data from a conductance probe, in the form of time traces and PDF plots, were used to identify flow regimes. From the void fraction time trace and PDF plots, Costigan and Whalley (1997) provided a set of criteria for flow regime determination.

To date, very little effort has been done to find an objective method of determining the microgravity two-phase flow regimes and their transitions. Reported microgravity flow regimes by Bousman et al. (1996), Rezkallah and Zhao (1995), Colin and Fabre (1995), Zhao and Rezkallah (1993), and Dukler et al. (1988) used video recordings or photographic images to determine flow regime. In the study of Bousman et al. (1996), film thickness time traces were used in conjunction with video images to identify the flow. However, the identifications were still largely subjective, and often relied on video images.

A preliminary study was done by Elkow and Rezkallah (1997) to use the void fraction PDF plots to characterize the behavior of gas–liquid flows under microgravity conditions. Flow regime characterizations that are peculiar to the reduced gravity environment were successfully outlined in that study. It was found, however, that the void fraction sensor used was too long (10 tube diameters), and that higher sampling rates were also needed.

It is the objective of this research to build a "short" sensor for measuring void fraction in two-phase flow, and to use this sensor to acquire microgravity void fraction data. A second objective is to use the void fraction time traces and PDF plots to develop a more objective method of flow regime identification for microgravity two-phase flow. The final objective is to test and compare flow regime transition models presented in the literature using the new data set.

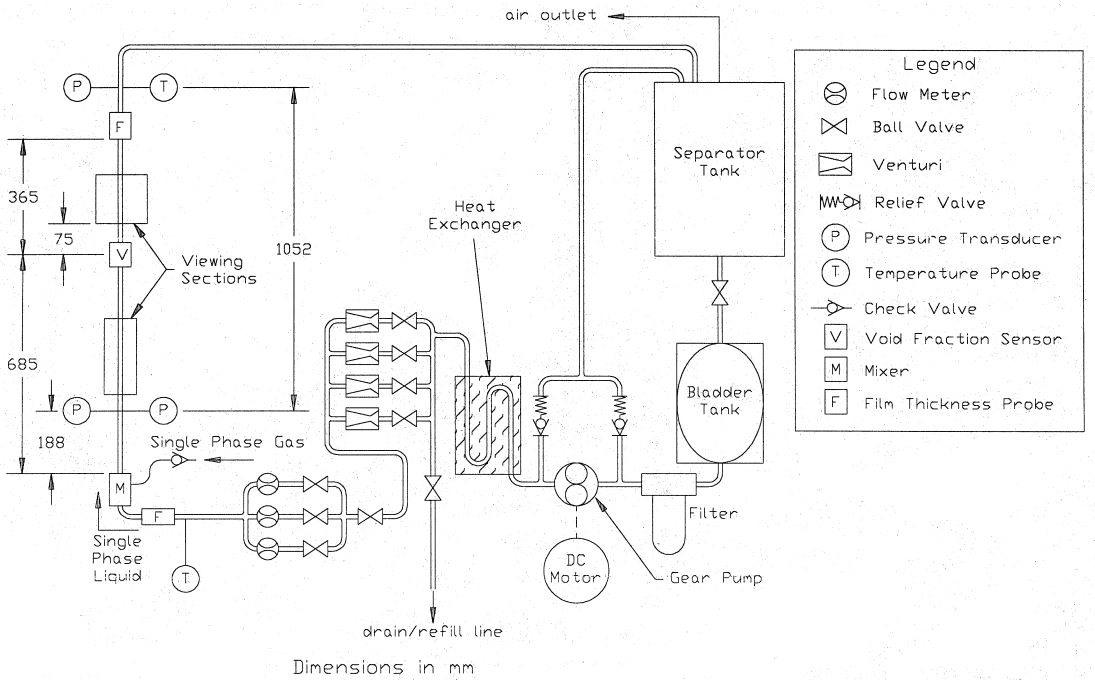

Fig. 2. A schematic diagram of the two-phase flow apparatus.

2. Experimental apparatus

A two-phase flow apparatus was previously developed to acquire data in vertical upward two-phase flow at normal gravity, and also at microgravity using the NASA Lewis DC-9 microgravity aircraft. A schematic diagram of the apparatus is shown in Fig. 2, and a brief description follows. A more detailed description can be found in Lowe (1997).

The 9.525 mm (3/8 in.) inner diameter test section begins with a mixer in which the liquid phase enters axially, and the gas phase enters radially through a number of small holes. Absolute pressure measurements are taken 188 mm (19.7 D) downstream of the mixer outlet. A viewing section is placed immediately after the absolute pressure probe for use with a Sony Hi-8 video camera. The center of the void fraction sensor is placed 685 mm (72 D) from the mixer and is followed by a viewing section for the NAC high speed video camera (1000 f.p.s.). Following the viewing section are two film thickness probes separated by 3 D, the first of which is located 105 mm (110 D) from the mixer.

Due to the limited space on the microgravity aircraft, and the large volume of liquid circulated during a series of experiments, it is necessary to recirculate the liquid phase. In order to do this, a two-stage separation system is used. During the first stage, the actual separation of the two phases takes place in a large tank and in the second stage, the liquid is drawn into a flexible bladder type tank for recirculation in the loop. A cutaway view of the separator tank is shown in Fig. 3. It is designed to first dissipate the inertia of the flow mixture, and then to trap the liquid while allowing the gas to escape, a difficult task to accomplish in the absence of gravity. Dissipation of the flow inertia is achieved by allowing the flow mixture to enter

tangential to the tank wall with an approximately 30° down inclination. The flow energy is then dissipated through wall friction as it flows around the circumference of the tank. In addition, the downward inclination of the inlet tube directs the liquid phase towards a nylon screen which covers a stainless steel mesh that fills the bottom third of the separation tank. The nylon screen and the stainless steel mesh effectively trap the liquid at the bottom of the tank by surface tension. The gas phase is allowed to escape through the center of the tank lid. In order to prevent liquid loss (since there may still be droplets of liquid floating in the tank), the air outlet is surrounded by a baffle and covered with a 1 mm by 1 mm Nylon screen, as shown in Fig. 3. After leaving the separation tank, the gas phase passes through another tank filled with water absorbing material before it is allowed to vent into the aircraft cabin.

The second stage of separation is to draw the liquid phase from the separator tank for recirculation. To ensure complete separation of the phases, this is done only during the high gravity (1.8 g) portion of the flight. Immediately after the plane enters the high-g portion of the parabola, a ball valve at the bottom of the separator tank is opened to allow the liquid to gravity feed into a specially designed flexible bladder tank. The latter is designed such that as the liquid is pumped out of the tank, it will collapse on itself. This prevents air from entering the tank, or a failure due to the large negative pressure that would be caused by the removal

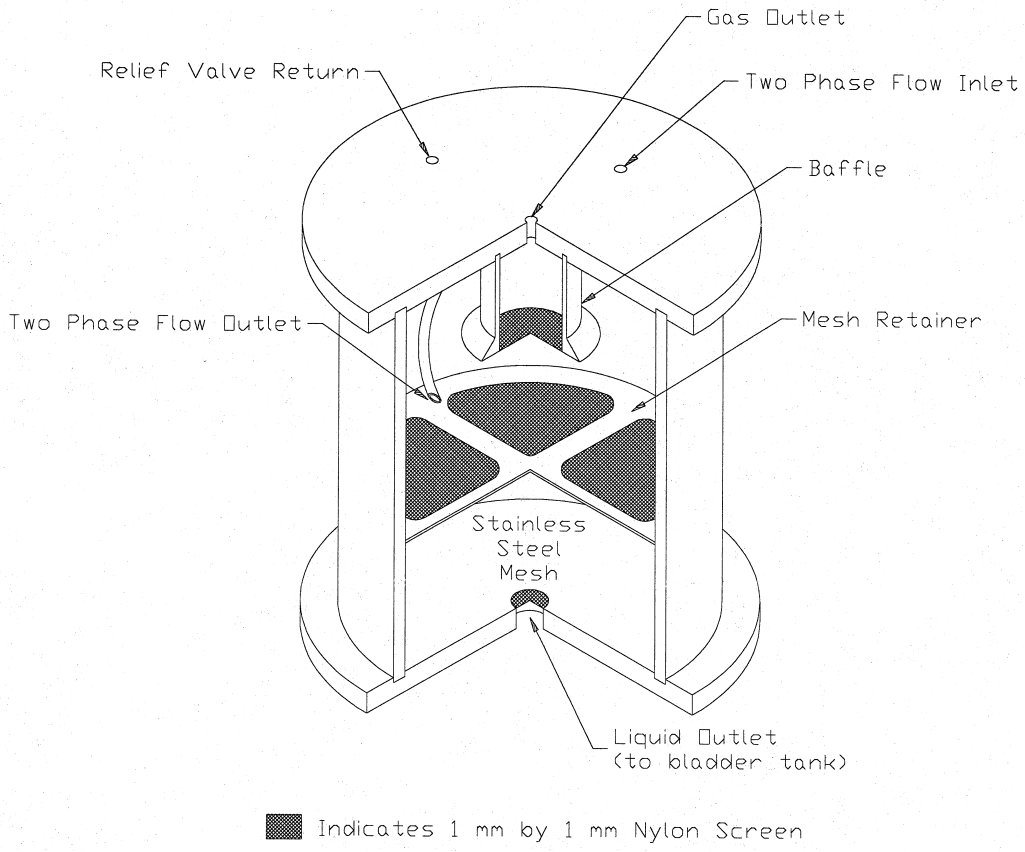

Fig. 3. Cutaway of separator tank (stainless steel mesh omitted for clarity).

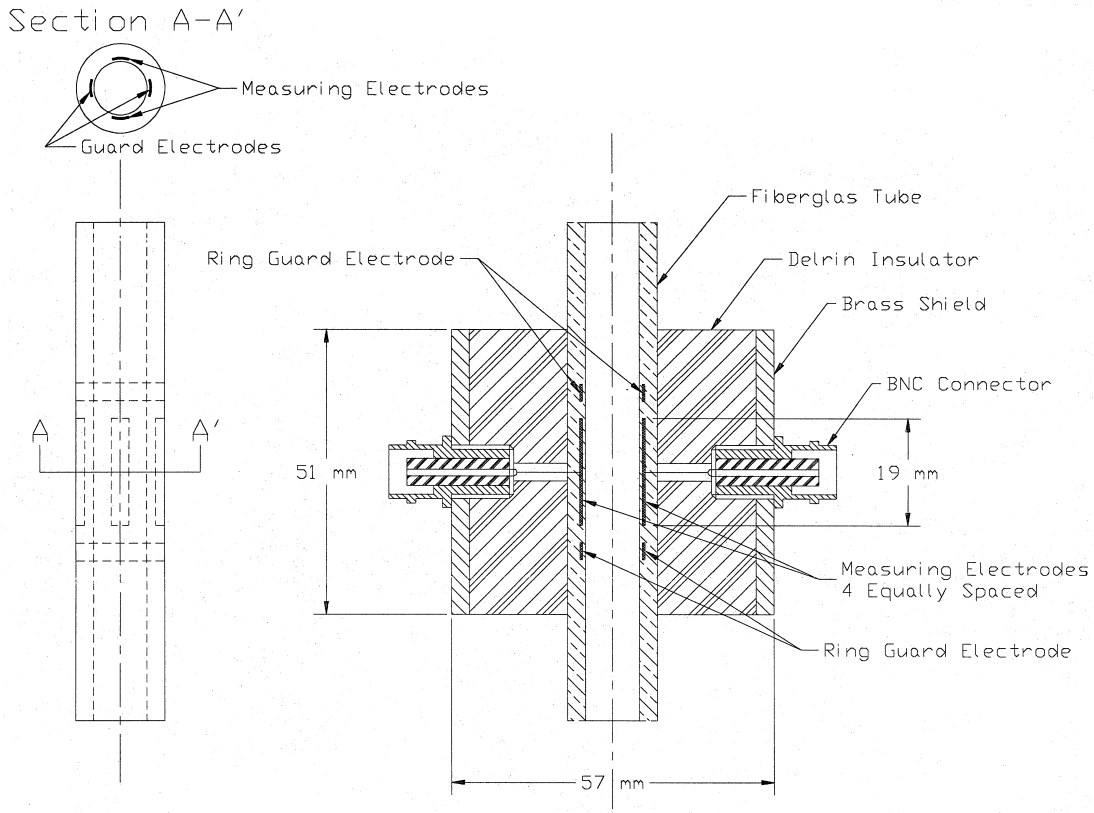

Fig. 4. Schematic diagram of capacitance void fraction sensor.

of water from a rigid tank. This separation process ensures that only single phase liquid is contained in the bladder tank which feeds the gear pump for recirculation.

A gear pump moves the single phase liquid from the bladder tank to a heat exchanger and a combination of four differently sized venturis before entering one of three manually selected turbine flow meters. The superficial liquid velocity (U_{SL}) is controlled by adjusting the pump speed using a dc motor, and selecting suitable venturi combinations. Each flow rate is set prior to the microgravity portion of each parabola. Single phase gas is supplied to the mixer from either a compressed air cylinder (provided onboard the NASA DC-9) or an air compressor (during ground tests). The superficial gas velocity (U_{SG}) is set by a computer controlled air mass flow controller.

A short capacitance sensor, shown schematically in Fig. 4, was designed and built to measure the volumetric void fraction. The sensing element length is 2 D (geometrical length), and it was chosen as a compromise between the greater sensitivity obtained with a longer sensor, and the ability to measure small fluctuations in the flow with a shorter one. Calibration of the void fraction sensor was performed using quick closing gate valves and a ground calibration loop. The calibration showed a correlation coefficient squared (R^2) of 0.998, and a precision error of 0.022 with a 95% confidence level. The calibration line was linear for void fractions between 0.06 and 0.88. The time constant of the measuring circuit was 10 μs,

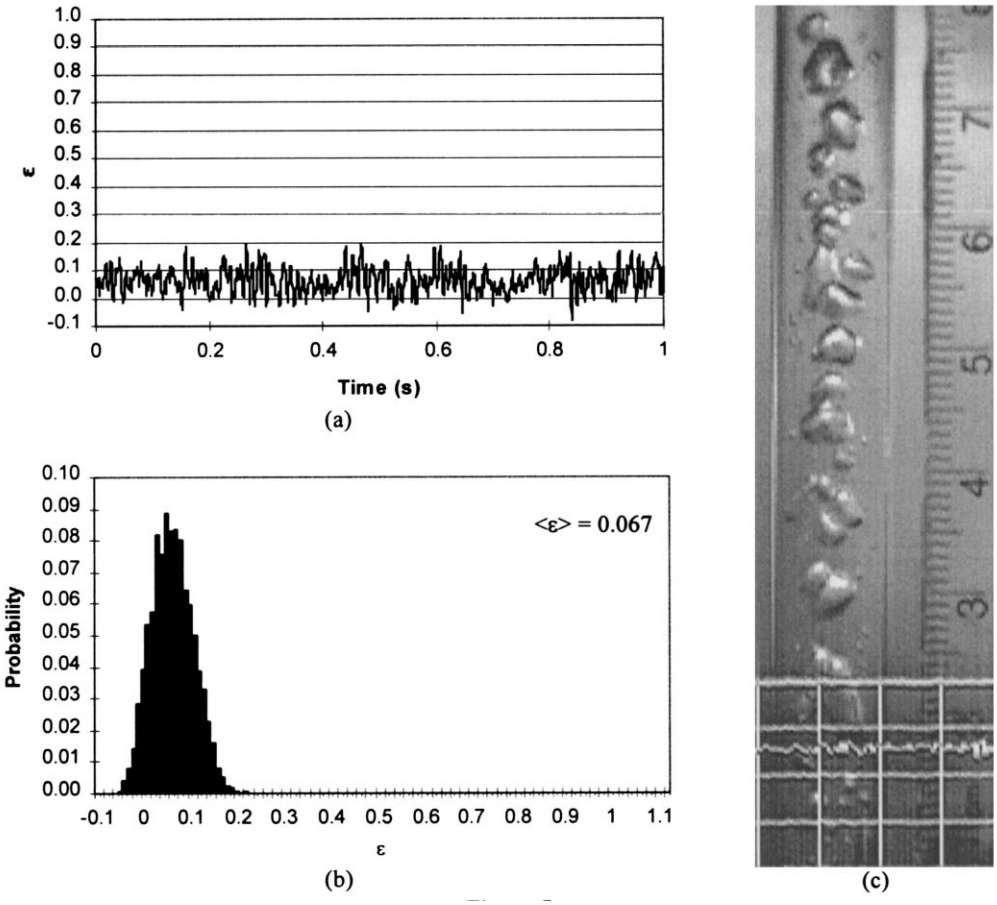

Fig. 5. Bubbly flow, U_{SL} = 2.53 m/s and U_{SG} = 0.196 m/s, showing: (a) time trace; (b) PDF; and (c) flow image.

corresponding to a dynamic response of 100 kHz. Analysis of FFT tests showed that all major flow fluctuations were below 100 Hz, thus the response time of the sensor was more than adequate.

The film thickness was measured using two probes separated by a tube length of 3 D. These probes were constructed with two thin wires strung across the tube diameter. Each wire was insulated from the wall to the tube centerline on one end, and was in contact with the flow on the other end. The conductance between the two wires was then measured and compared to values obtained from calibration to determine the liquid film thickness near the wall.

The void fraction and film thickness data were recorded at 1024 Hz using a 486/66 MHz computer with a 12 bit analog to digital converter. Another 486/66 MHz computer recorded and displayed at approximately 70 Hz, gas and liquid flow rates, pressures, temperatures, pump speed, and gravity levels in the x, y, and z directions with a 12 bit analog-to-digital converter.

3. Typical flow regime identifiers

This section presents typical void fraction time traces and their PDF along with video images for the four flow regimes. Each flow regime is clearly identified from video images, and none of the flow set points in Figs. 5–8 fall near a transition area. It should be noted that the negative void fraction values shown on some of the PDF plots are a result of noise in the void fraction signal which had not been removed by filtering. The complete void fraction data set is presented in Table 1, with the flow settings discussed in the following sections marked with an asterisk. All the data presented was collected when the gravity level in all three directions was between ± 0.03 g. The void fraction data for each flow setting was collected at 1024 Hz between 4 and 20 s.

3.1. Bubbly flow

Bubbly flow is characterized by the time trace and PDF as typically shown in Fig. 5(a) and (b). Also shown in Fig. 5(c) is an image grabbed from the high speed video system which

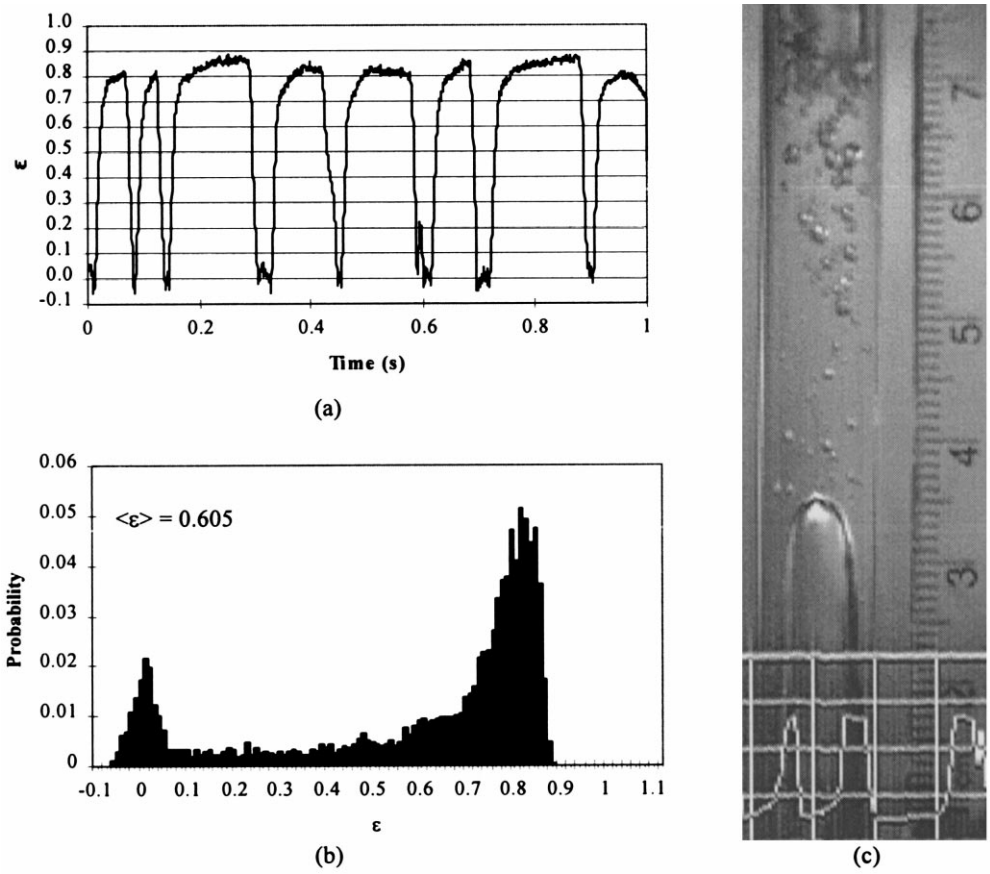

Fig. 6. Slug flow, $U_{SL} = 0.42$ m/s and $U_{SG} = 0.99$ m/s, showing: (a) time trace; (b) PDF; and (c) flow image.

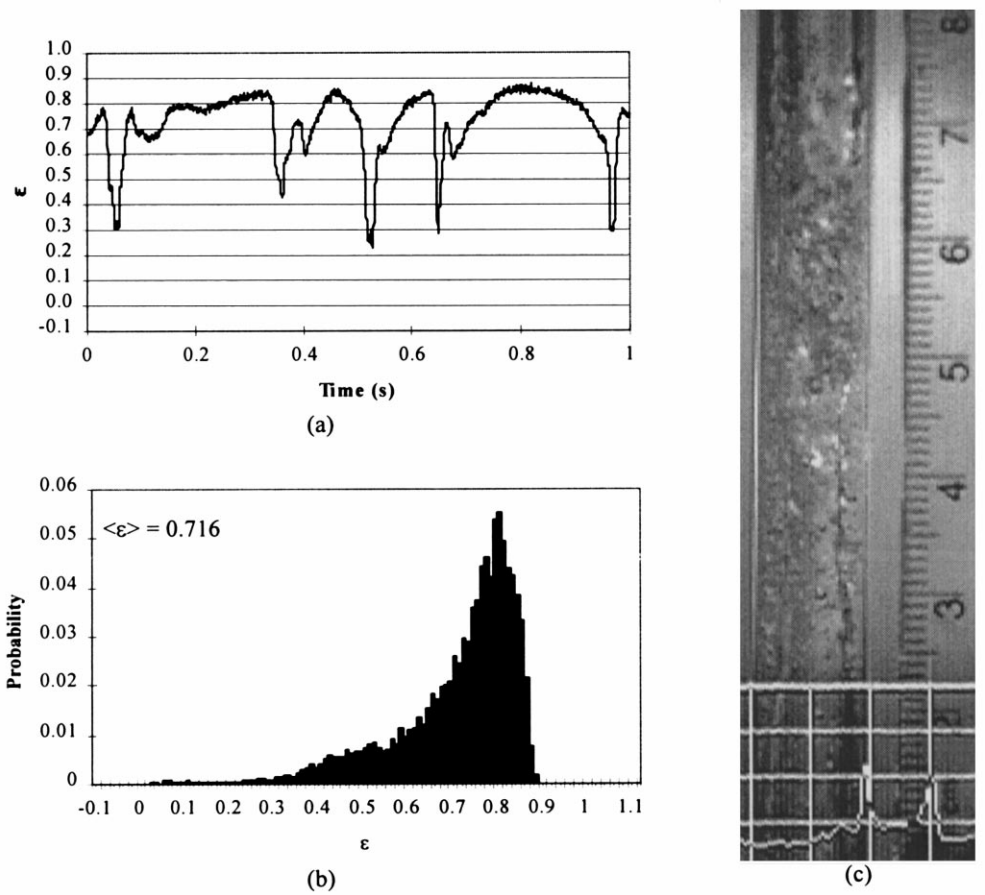

Fig. 7. Transitional flow, U_{SL} = 0.25 m/s and U_{SG} = 2.98 m/s. showing: (a) time trace; (b) PDF; and (c) flow image.

clearly shows distinct bubbles flowing at the centerline of the tube. The void fraction time trace centers around a low average void fraction with small fluctuations corresponding to the passage of the bubbles. The PDF for bubbly flow has a single narrow peak at a low void fraction, indicative of the small fluctuations about a mean value. It was found that a PDF with a single peak at a void fraction typically less than 0.2 corresponds to bubbly flow.

3.2. Slug flow

A void fraction time trace, its PDF, and the flow image for a typical slug flow are shown in Fig. 6. The time trace for a slug flow is characterized by a void fraction signal which fluctuates between high and low values. The high void fraction corresponds to the passage of a Taylor bubble, while the low void fraction indicates the passage of a liquid slug. The flow image in Fig. 6(c) shows the passage of a liquid slug, with the tail of the preceding Taylor bubble exiting at the top and the nose of the next Taylor bubble entering at the bottom of the viewing section. The small bubbles at the tail of the exiting bubble are the result of a small amount of slip between the liquid and gas induced at higher gas velocities. The slug flow PDF has two

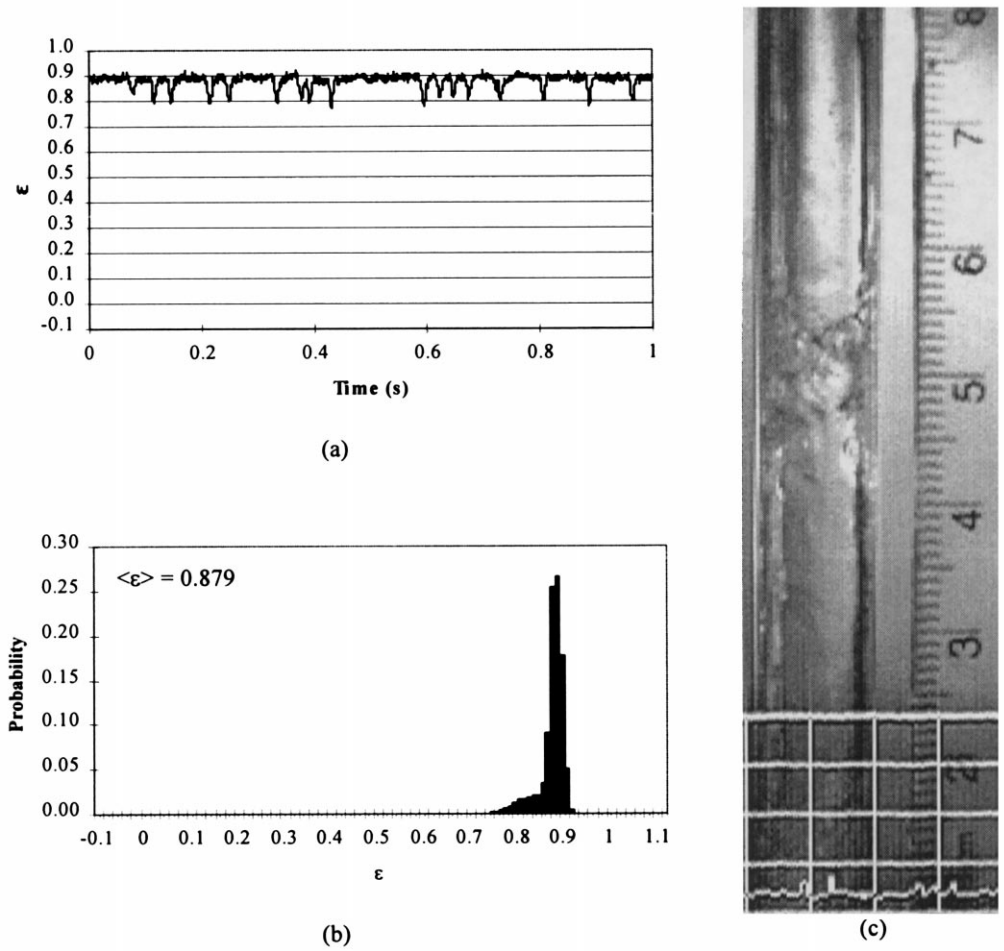

Fig. 8. Annular flow, $U_{SL} = 0.07$ m/s and $U_{SG} = 20.94$ m/s, showing: (a) time trace; (b) PDF; and (c) flow image.

peaks, one at a high void fraction and the other at a low void fraction corresponding to the passage of Taylor bubbles and liquid slugs, respectively.

3.3. Transitional flow

The transitional flow regime is typically characterized by the void fraction time trace and PDF shown in Fig. 7(a) and (b). Also shown in Fig. 7(c) is a typical image of the unstable frothy slug region which characterizes transitional flow. The void fraction time trace of a transitional flow tends to stay at a high void fraction with random dips into lower void fractions. Typically, these lower void fraction dips are very short lived, indicating the unstable nature of the slug. The PDF for this flow regime shows a single broad peak, with the maximum typically between a void fraction of 0.7 and 0.9, with a long tail extending down to void fractions as low as 0. The single peak in the PDF at high void fraction reflects the

Table 1
Microgravity air–water void fraction data[1]

Flow regime	U_{SL} (m/s)	U_{SG} (m/s)	$\langle\varepsilon\rangle$	Flow regime	U_{SL} (m/s)	U_{SG} (m/s)	$\langle\varepsilon\rangle$	Flow regime	U_{SL} (m/s)	U_{SG} (m/s)	$\langle\varepsilon\rangle$	Flow regime	U_{SL} (m/s)	U_{SG} (m/s)	$\langle\varepsilon\rangle$
B	1.72	0.10	0.074	S	0.26	0.89	0.666	T	0.04	4.92	0.829	T/A	0.31	11.92	0.796
B	1.79	0.20	0.107	S	0.26	1.29	0.684	[2]T	0.06	4.97	0.814	A	0.05	6.92	0.855
B	1.78	0.40	0.161	S	0.25	1.69	0.700	T	0.09	4.92	0.799	A	0.04	8.91	0.864
B	2.53	0.10	0.044	S	0.25	1.99	0.686	T	0.09	6.93	0.815	A	0.04	10.91	0.873
[2]B	2.53	0.20	0.067	S	0.25	1.68	0.689	[2]T	0.11	1.59	0.724	A	0.03	12.91	0.885
B	2.53	0.39	0.110	S	0.43	0.29	0.373	T	0.12	2.18	0.750	A	0.05	14.92	0.882
B	2.51	0.49	0.126	S	0.42	0.49	0.495	T	0.11	2.48	0.754	A	0.05	16.95	0.885
B	2.51	0.59	0.145	S	0.42	0.69	0.541	T	0.11	2.78	0.761	A	0.05	18.95	0.888
B	3.03	0.10	0.031	[2]S	0.42	0.99	0.605	T	0.16	1.89	0.740	A	0.05	20.94	0.889
B	1.73	0.20	0.106	S	0.42	1.19	0.633	T	0.15	2.18	0.744	[2]A	0.06	8.92	0.838
B	2.49	0.10	0.043	S	0.43	1.98	0.659	T	0.15	2.48	0.743	A	0.08	10.96	0.858
B	2.49	0.20	0.065	S	0.72	0.49	0.342	T	0.15	2.78	0.736	A	0.08	12.91	0.860
B	2.52	0.30	0.088	S	0.72	0.59	0.381	T	0.16	3.95	0.755	A	0.08	14.92	0.860
B	2.52	0.40	0.109	S	0.72	0.69	0.402	T	0.16	3.96	0.764	A	0.08	16.90	0.869
[2]B	2.51	0.59	0.145	S	0.73	0.79	0.424	T	0.16	5.96	0.790	A	0.09	9.96	0.840
B	0.43	0.19	0.278	S	0.72	1.09	0.494	T	0.22	2.96	0.720	A	0.08	12.95	0.857
B	0.74	0.09	0.148	S	1.01	1.99	0.525	T	0.22	4.95	0.761	A	0.08	14.96	0.865
B	0.73	0.20	0.209	S	1.01	2.48	0.549	T	0.20	6.92	0.781	A	0.07	16.95	0.871
B/S	1.72	0.40	0.164	S	1.00	2.98	0.567	T	0.20	8.93	0.798	A	0.07	18.95	0.875
B/S	1.78	0.50	0.184	S	1.71	0.49	0.188	T	0.26	2.28	0.709	[2]A	0.07	20.94	0.879
[2]B/S	2.51	0.79	0.174	S	1.71	0.59	0.209	T	0.26	2.58	0.699	A	0.11	9.92	0.830
B/S	2.51	0.79	0.174	S	1.71	0.79	0.245	[2]T	0.25	2.98	0.716	A	0.11	11.91	0.845
S	0.10	0.79	0.733	S	1.70	0.99	0.279	T	0.25	3.78	0.736	A	0.11	13.96	0.853
[2]S	0.10	1.09	0.756	S	1.71	1.19	0.311	T	0.31	1.95	0.679	A	0.11	15.91	0.860
S	0.11	0.19	0.565	S	1.77	0.59	0.202	T	0.31	3.96	0.720	A	0.10	19.89	0.874
S	0.12	0.29	0.607	S	1.77	0.79	0.241	T	0.31	5.92	0.738	A	0.11	17.91	0.869
S	0.12	0.40	0.658	S	1.77	0.99	0.273	T	0.30	7.95	0.765	A	0.11	19.91	0.859
S	0.12	0.49	0.713	S	1.77	1.19	0.303	T	0.32	9.91	0.781	A	0.15	11.96	0.829
S	0.17	0.78	0.717	[2]S	2.50	0.99	0.200	T	0.40	2.98	0.676	A	0.15	13.96	0.838
S	0.15	1.09	0.726	S	2.50	1.19	0.224	T	0.40	3.48	0.689	A	0.15	15.96	0.846
S	0.15	1.29	0.720	S	2.50	1.19	0.225	[2]T/A	0.06	6.92	0.831	A	0.15	17.91	0.855
S	0.24	0.19	0.383	[2]S/T	0.10	1.29	0.743	T/A	0.09	7.94	0.826	A	0.15	19.90	0.862
S	0.22	0.29	0.480	S/T	0.16	1.59	0.716	T/A	0.09	7.91	0.823	A	0.20	11.96	0.816
S	0.22	0.49	0.605	S/T	0.40	2.48	0.665	T/A	0.16	7.96	0.807	A	0.21	13.95	0.828
S	0.22	0.69	0.620	S/T	1.00	3.48	0.590	T/A	0.16	9.94	0.815	A	0.20	15.95	0.838
S	0.22	0.89	0.719	S/T	1.00	3.98	0.596	T/A	0.20	10.92	0.811	A	0.31	13.92	0.809
												A	0.31	15.92	0.818

[1]Absolute pressure was 89 ± 3 kPa and mixture temperature was $21.5 \pm 1.5^{\circ}$C.[2]Indicates flow settings used in plotting Figs. 5–12

proximity of this transition to annular flow, and the long tail represents the passing of short unstable slugs.

3.4. Annular flow

Annular flow is typically represented by the void fraction time trace and PDF shown in Fig. 8. The void fraction time trace for annular flow remains constant at a value typically between 0.80 and 0.90. Fig. 8(c) shows that the liquid film is occasionally interrupted by the passing of disturbance waves. The "foot print" of such waves is shown in the time trace as small dips into lower void fractions. A typical PDF for annular flow has a very narrow peak at a void fraction between 0.80 and 0.90, with a short tail extending into lower void fractions. The narrow peak in the PDF indicates that the film maintains a nearly constant thickness between the passing of disturbance waves.

Void fraction data was recorded for flow settings covering all of the flow regimes described above and the results are plotted with those of Elkow (1995) and Bousman (1995) in Fig. 9.

4. Transitions

The PDF plots presented in the previous sections show clear differences between each flow regime. However, as the flow approaches a transition region between two distinct flow regimes, the differences between the PDF plots become more subtle. Regardless, it was found that the PDF still showed well identified differences between the flow regimes close to a transition. Since the transitions between flow regimes take place over a range of flow settings, flows which

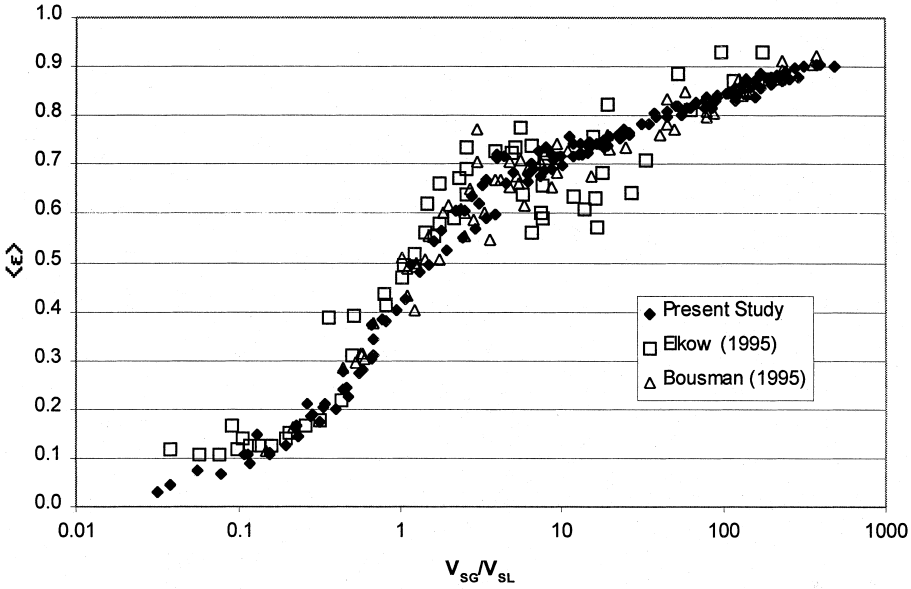

Fig. 9. Comparison of void fraction data with Elkow (1995) and Bousman (1995).

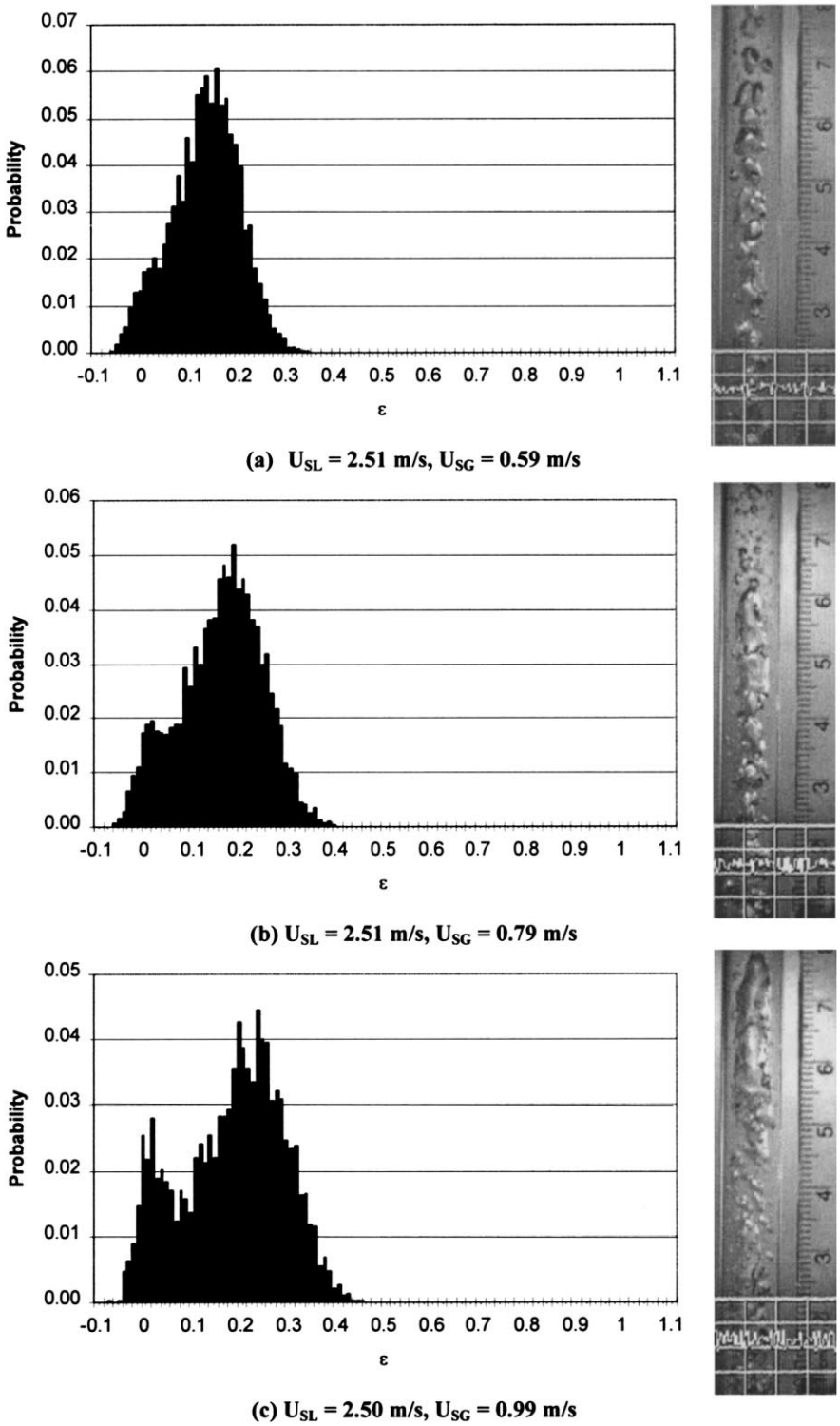

Fig. 10. Bubbly-to-slug void fraction PDF plots and flow images: (a) bubbly; (b) bubbly/slug; and (c) slug.

displayed characteristics of two neighboring flow regimes were labeled as both flow regimes (e.g. bubbly–slug or B/S). In the following discussion, PDF plots and corresponding video images are presented for the flow just before a transition, during a transition, and after a transition.

4.1. Bubbly-to-slug

The bubbly-to-slug transition takes place when small (typically less than 1 D) discrete bubbles begin to pack together and flow in clusters. This leads to coalescence and the formation of Taylor bubbles which characterize slug flow. While both bubbly and slug flows are usually easy to identify from the video images, the subjectivity of the observer can often introduce a bias in determining where the transition between the two regimes actually occurs.

Fig. 10 shows how the void fraction PDF changes as the flow transitions from bubbly to slug flow, and the flow images corresponding to each flow setting. Fig. 10(a) is a bubbly flow; as can be clearly seen in the flow image. The PDF in Fig. 10(a) is that of a typical bubbly flow with a single peak at a void fraction of less than 0.20 (approximately 0.16). In Fig. 10(b), the gas flow rate was increased, and the flow is now in a transition from bubbly to slug flow. The video image of this flow setting shows the formation of bubbles which are approaching 1 D in length, and the bubbles are beginning to flow in clusters separated by slugs of water with fewer bubbles. The PDF for this flow setting is much like that of a bubbly flow, with the exception that a second peak is beginning to form at a void fraction slightly above zero. The start of the second peak near zero indicates that the bubbles are beginning to flow in clusters separated by slugs of liquid that contain some bubbles. Note also that the main peak is now at a void fraction of about 0.2, indicating larger and more closely packed bubbles.

A further increase in the gas flow rate results in the PDF and flow image shown in Fig. 10(c). At this flow setting, the flow has transitioned into slug flow, and the video image clearly depicts a short Taylor bubble ($L \approx 2.5$ D) near the top of the viewing section. The PDF has now taken on the two definite peaks that are characteristic of slug flow, one at a void fraction of about 0.02, and the second at approximately 0.25.

4.2. Slug-to-transitional flow

The transition from slug to transitional flow is often very difficult to determine from flow images alone; hence visual identification is quite subjective. The transition occurs when the gas phase flowing in Taylor bubbles begins to reach a high enough inertia to temporarily break through some of the liquid slugs separating the Taylor bubbles. The liquid phase quickly recovers to form another slug, which is then broken again by the incoming gas phase. As the gas flow rate is further increased, more slugs become unstable and transitional flow occurs.

Fig. 11 shows how the void fraction PDF changes as the flow develops from slug into transitional flow. Slug flow is depicted in Fig. 11(a), with a clear liquid slug between the tail of a Taylor bubble and the nose of a consecutive one. The PDF for this flow setting clearly shows the double peaks which characterize slug flow. The fact that the peak at the high void fraction is very narrow and reaches a relatively high probability indicates that the Taylor bubbles are very long and smooth, as can be seen from examination of the video images. The small peak at

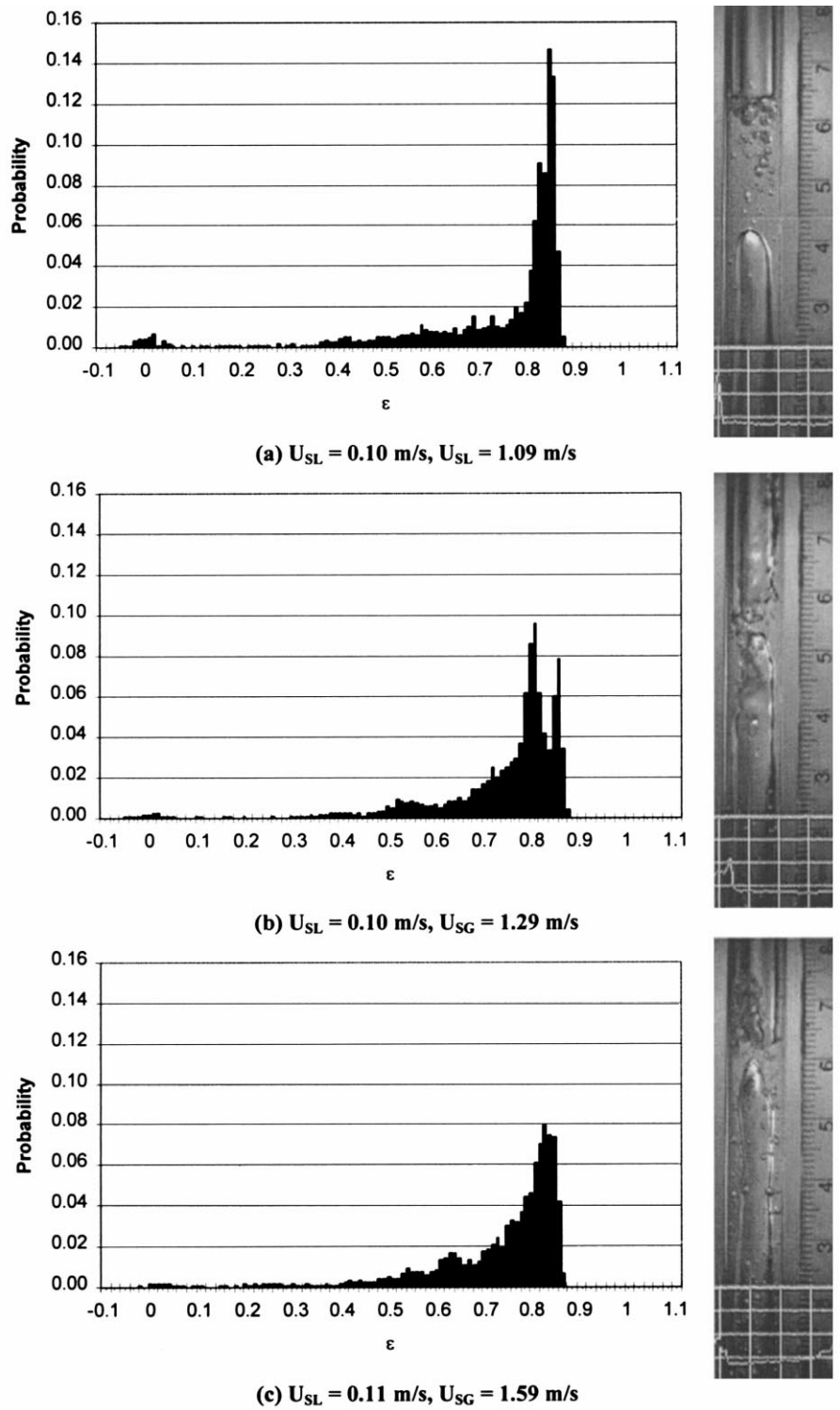

Fig. 11. Slug-to-transitional void fraction PDF plots and video images: (a) slug; (b) slug/transitional; and (c) transitional.

the low void fraction of about 0.02 indicates that the liquid slugs are short with few entrained bubbles; this is clearly shown in the video images of Fig. 11.

Fig. 11(b) is a setting which shows characteristics of both slug and transitional flows. The video image shows a distorted slug about to be destroyed by the bubble behind it. However, there are just as many cases in the video where, what appears to be a stable slug, passes through the viewing section. The PDF for this flow shows characteristics of both flow regimes. It has a broad peak at a high void fraction, with a long tail into low void fractions, which is characteristic of transitional flows. However, there is still a small peak at a void fraction of 0.03 indicating that there are still some stable slugs passing through the sensor.

Fig. 11(c) shows the result of increasing the gas flow rate slightly, resulting in transitional flow. The video image shows a bubble about to burst through an unstable slug, while the PDF is that of a typical transitional flow. The latter has a single peak at a void fraction of about 0.84, with a long tail extending into void fractions as low as zero. The peak at the low void fraction which was clearly seen in Fig. 11(a) and (b) is no longer distinguishable. Instead, a long flat tail extends to low values of void fraction, which is typical of transitional flows.

4.3. Transitional-to-annular

The transition to annular flow is recognized when the unstable slugs of a transitional flow no longer bridge the tube and instead become more of a disturbance wave on the annular film. The transition is complete when the liquid flows as a film on the wall, typical of annular flow, occasionally interrupted by large amplitude waves that do not completely bridge the tube. The transition is the most difficult to identify from video images, especially at high liquid flow rates. The unstable slugs and disturbance waves are often very frothy due to the presence of entrained gas bubbles in the film and liquid "froth" in the gas core, making it quite difficult to determine the inner features of the flow.

Fig. 12 shows the void fraction PDF plots and the video images for a transition to annular flow. The video image in Fig. 12(a) shows the passage of an unstable slug with liquid bridging. The corresponding PDF shows a sharp peak at a high void fraction due to the mainly annular nature of the flow, with a tail that extends to a void fraction of 0.45. The significance of where the tail of the PDF stops will be discussed later in this section.

Fig. 12(b) is from a flow setting that falls on the boundary between transitional and annular flow. Thus, it contains many of the features of both flows. The video image shows the passage of what appears to be a distorted slug, but it is difficult to determine if the bridging is complete. However, examination of the video tape for this flow setting shows other instances where bridging is likely not complete, as well as several other images where bridging did occur. The PDF for this flow setting shows a slightly higher peak at the high void fraction, indicating the more annular nature of this flow than the previous one, with a tail extending down to a void fraction of about 0.49.

Fig. 12(c) shows the result of increasing the gas flow rate further. The video image clearly shows the passing of a wave on the annular film, and in this case it is clear that the wave does not bridge the tube. The PDF for this flow setting is similar to the previous ones, with a slightly higher peak and a tail extending to a void fraction of about 0.53.

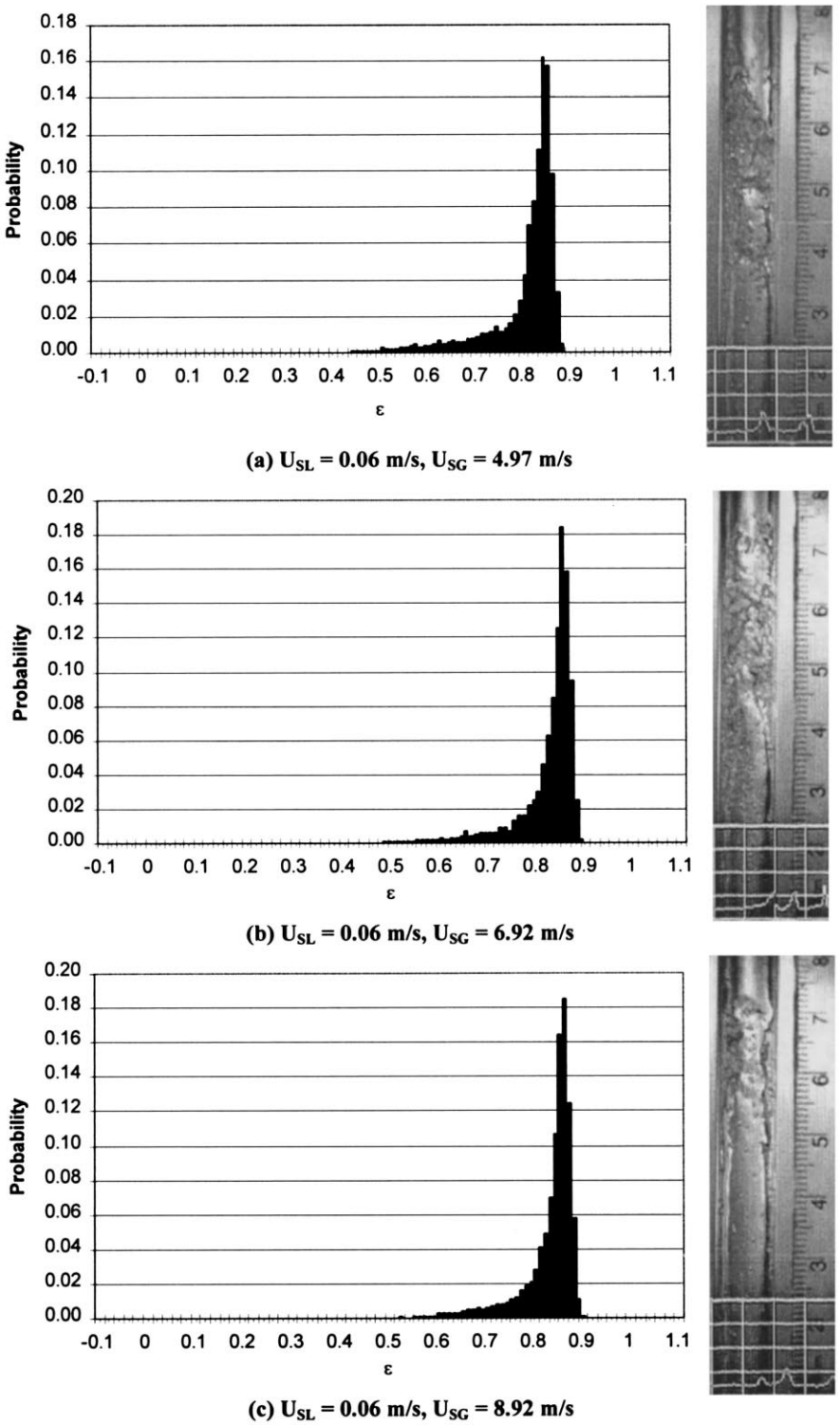

Fig. 12. Transitional-to-annular void fraction PDF plots and video images: (a) transitional; (b) transitional/annular; and (c) annular.

After examining the PDF plots in Fig. 12, it is clear that they more or less resemble each other. However, there is one feature that does offer a method of determining the flow regime without the aid of the video. This is associated with how far into lower void fractions the PDF tail extends. Such low values correspond to the passing of disturbances, be they waves on the annular film or unstable slugs/bridging events. Thus, it is the tail of the PDF which gives some clue as to which flow regime is present in the tube by allowing determination of the void fraction at which an unstable liquid slug can no longer bridge the tube and evolves into a disturbance wave. This, of course, is not expected to occur at a single value of void fraction but instead it occurs over a small range during which the transition actually takes place.

Re-examining Fig. 12, it is clear that when the PDF tail reaches a void fraction below 0.45, transitional flow exists, and when the tail does not extend past 0.50, annular flow exists. It could then be argued that the transition to annular flow takes place when the PDF tail stops somewhere between 0.45 and 0.50. This conclusion is obviously not based on one set point. Examination of PDF plots and video recordings of several other flow settings (see Lowe, 1997) also seem to give similar results.

In an attempt to explain why the transition would occur when the void fraction in the slugs is between 0.45 and 0.50, consider the case of a liquid slug containing many small bubbles. To determine where the transition from bubbly to slug flow exists, Dukler et al. (1988) pointed out that the maximum void fraction that small spherical bubbles arranged in a cubic array can achieve is 0.52. For larger bubbles of non-spherical shape, the maximum void fraction drops to approximately 0.40. Dukler et al. (1988) speculated that the transition from bubbly to slug flow occurs at a void fraction of about 0.45. Thus, for a disturbance passing the void fraction sensor to be registered as a bridging event (i.e. a short slug), it must have a void fraction of less than 0.52 if it contains small bubbles. On the other hand, if the bridging event contains larger bubbles, then the void fraction must be below 0.4. If the void fraction PDF plot does not show values below 0.52, then it can be argued that a complete bridging must not have occurred, and that annular flow thus exists. One could then conclude that a transitional flow, characterized by many bridging events, could only occur when the tail of the PDF plot extends below 0.45, and that annular flow would occur when the lowest ε value on a PDF plot remains above 0.50.

Since the void fraction sensor measures a volumetric void fraction over a tube length of 2 D, it is possible that disturbances shorter than 2 D will not be properly represented in the PDF. To check this possibility, two things were done. First, the video images were reviewed to determine the typical length of a disturbance in the transitional and annular flow regimes (see Fig. 12). It was found that the majority of the disturbances were about 2 D in length. Secondly, the PDF plots of the film thickness measurement were examined to ensure that short slugs were not improperly represented by the void fraction PDF. Since the film thickness is a local measurement, it will pick up even the shortest slug or bridging event. Details on the film thickness sensors can be found in Rezkallah and de Jong (1998).

Fig. 13 shows the film thickness PDF plots corresponding to the flow settings shown in Fig. 12. It is clear that none of these PDF plots show a histogram that extends all the way to 4.76 mm (half the tube diameter), indicating that a complete liquid bridging did not occur. The probes are, however, sensitive to bubbles that are trapped in the liquid film, and thus will indicate a thinner film thickness than what is actually there (if bubbles are present in the liquid

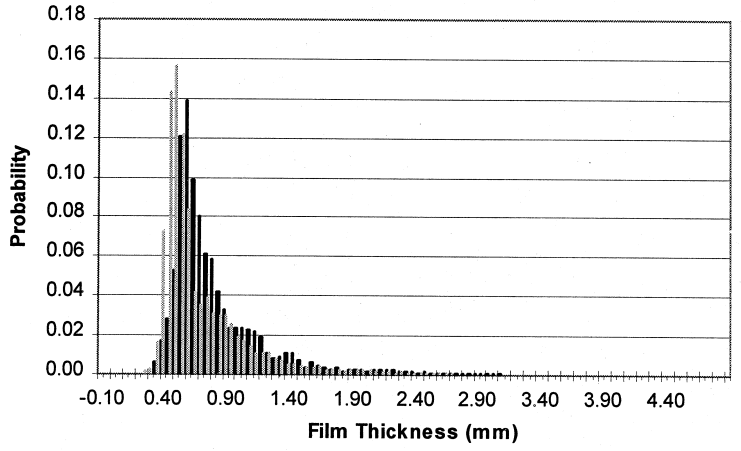

(a) U_{SL} = 0.06 m/s, U_{SG} = 4.97 m/s

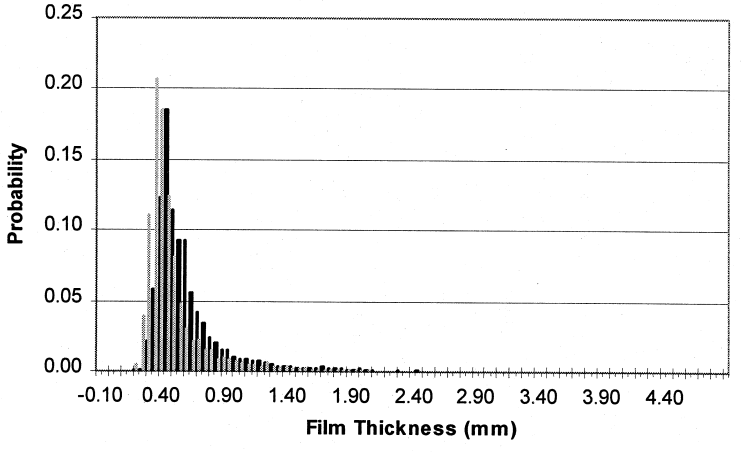

(b) U_{SL} = 0.06 m/s, U_{SG} = 6.92 m/s

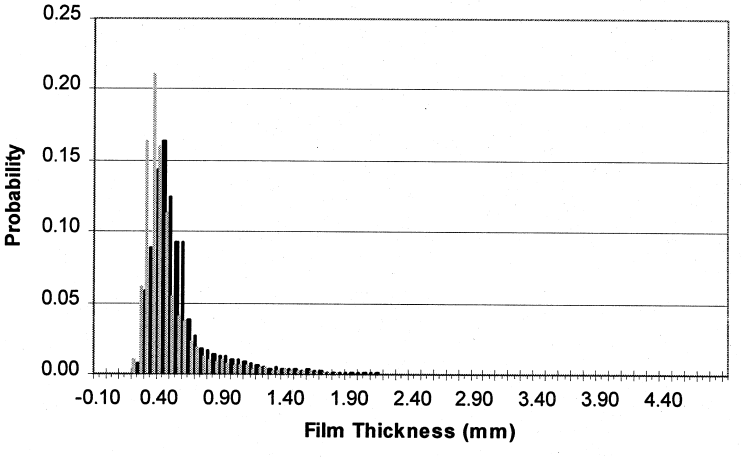

(c) U_{SL} = 0.06 m/s, U_{SG} = 8.92 m/s

Fig. 13. Transitional-to-annular film thickness PDF plots: (a) transitional; (b) transitional/annular; and (c) annular. ■ probe 1, □ probe 2.

film). Therefore, some compensation for the void fraction in the disturbance waves must be made. This compensation is as follows:

$$\delta_{\text{meas.}} = \delta_{\text{actual}}(1 - \varepsilon), \tag{1}$$

where δ_{actual} is the actual film thickness including bubbles, $\delta_{\text{meas.}}$ is the measured film thickness, and ε is the void fraction between the probes. While the void fraction between the probes is not directly measured, we can make some assumptions as to how the void fraction will affect the measurement.

Fig. 14 depicts the passage of several waves with various combinations of void fraction and film thickness. In Fig. 14(a), a pure liquid wave passes the sensor, so δ_{actual} is equal to δ_{measured} at 4.76 mm. If one makes the assumption that a disturbance covering half the tube diameter ($\delta_{\text{actual}} = 4.76$ mm) has the maximum void fraction for small closely packed bubbles ($\varepsilon = 0.52$; Dukler et al., 1988), as shown in Fig. 14(b), then Eq. (1) would give a measured film thickness of 2.28 mm. This assumption gives the minimum value the film thickness probes can read and still have bridging. Fig. 14(c) illustrates that if the film thickness is less than 2.28 mm, then the bridging can not be complete, even if the wave contains many bubbles. Disturbances with a void fraction less than 0.52 will have a film thickness between 2.28 and 4.76 mm, and may or may not bridge the tube depending on the void fraction; this is shown in Fig. 14(d) and (e).

If Fig. 13 is now re-examined, and a film thickness of 2.28 mm is considered to be where a bridging event occurs (i.e. the maximum film thickness reading for bridging not to occur), it can be seen that the transitional flow of Fig. 13(a) has a tail that extends well past 2.28 mm. This indicates that if the disturbances are frothy and contain packed small bubbles (as the video images show), bridging occurs. The PDF plots of Fig. 13(b) show a tail that extends to a film thickness at, or slightly past 2.28 mm, indicating that the events are bridging if the disturbances are very frothy. When the annular flow of Fig. 13(c) is examined, we see that the tail of the PDF remains below 2.28 mm, indicating that bridging is not complete even if the disturbances are at the maximum void fraction of 0.52.

Thus, it has been verified that transitional flow exists when the tail of the void fraction PDF extends below a void fraction of 0.45. Annular flow will exist when the void fraction PDF is completely contained at void fractions above 0.50. The transition between these two flow regimes happens when the tail of the void fraction PDF extends into the 0.45–0.50 range of void fraction.

5. Transition models

There are three predominant flow transition models in the literature for microgravity two-phase gas–liquid flows. The bubbly-to-slug model of Bousman et al. (1996) was based on the drift–flux model of Zuber and Findlay (1965). The gas drift velocity in the drift–flux model was set to zero, resulting in the following equation which relates the superficial velocities of both phases:

$$U_{\text{SL}} = \frac{(1 - C_0\langle\varepsilon\rangle)}{C_0\langle\varepsilon\rangle} U_{\text{SG}} \tag{2}$$

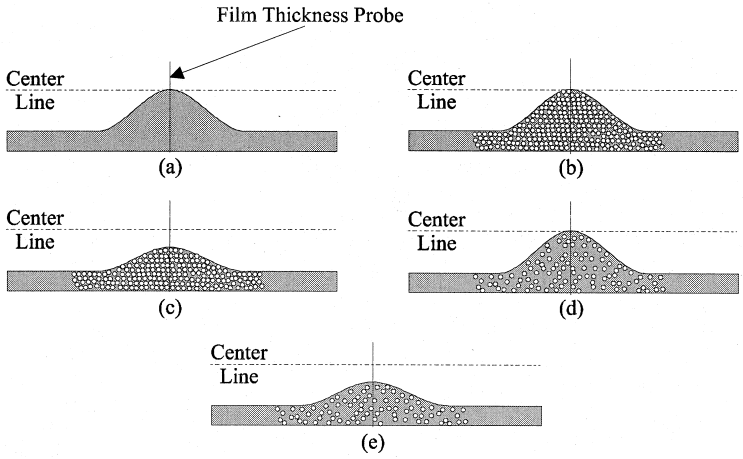

Fig. 14. Illustration of the effects of the presence of bubbles in the liquid film on film thickness measurements: (a) $\varepsilon_{wave} = 0$, $\delta_{measured} = \delta_{actual} = 4.76$ mm, bridging; (b) $\varepsilon_{wave} = 0.52$, $\delta_{measured} = 2.28$ mm, $\delta_{actual} = 4.76$ mm, bridging; (c) $\varepsilon_{wave} = 0.52$, $\delta_{measured} < 2.28$ mm $\delta_{actual} < 4.76$ mm, no bridging; (d) $\varepsilon_{wave} < 0.52$, $\delta_{measured} > 2.28$, $\delta_{actual} = 4.76$ mm, bridging; (e) $\varepsilon_{wave} < 0.52$, $\delta_{measured} < \delta_{actual} < 4.76$ mm, no bridging.

(Bousman et al., 1996). In Eq. (2), $\langle\varepsilon\rangle$ is the cross-sectional average void fraction, C_0 is the distribution coefficient, as defined by Zuber and Findlay (1965), and represents the radial distribution of the void and velocity profiles. A C_0 greater than 1 indicates a profile which is maximum at the center and minimum near the walls, while a C_0 less than 1 indicates a profile which peaks near the wall. A C_0 equal to 1 indicates uniform velocity and void profiles. Several experimental values of C_0 for water–air flows at microgravity have been reported in the literature, typically in the range of 1.20–1.30 for bubbly and slug flows. To complete the transition criteria set by Eq. (2), a transition void fraction is selected.

Fig. 15 is a dimensional flow pattern map in terms of liquid and gas superficial velocities. The current data set is plotted on the map and the bubbly-to-slug transition line is also plotted using a C_0 of 1.28 and a transition void fraction of 0.174. This line separates the bubbly and slug flows reasonably well, with only one bubbly flow point in the slug region. However, it was found that the transition line was very sensitive to C_0 and the value of the transition void fraction chosen. The latter varied considerably from one group to another, ranging from as low as 0.174 to as high as 0.45.

Two models for the slug-to-annular transition have been suggested. Dukler et al. (1988) and later Bousman (1995) proposed a void fraction matching slug-to-annular transition model. Bousman (1995) used a force balance approach to determine a void fraction relationship for annular flow and then equated this with a void fraction expression developed using the drift–flux model. Fig. 15 also shows the slug-to-annular transition line predicted from that model. As shown in the figure, this line is much less successful in predicting the slug-to-annular transition.

The Weber number transition model was suggested by Zhao and Rezkallah (1993) and later modified by Rezkallah (1996) to provide a dimensionless flow regime map based on the Weber number estimated from the liquid and gas velocities. In that model, it is argued that the dominant forces in microgravity two-phase flows are inertia and surface tension. The Weber

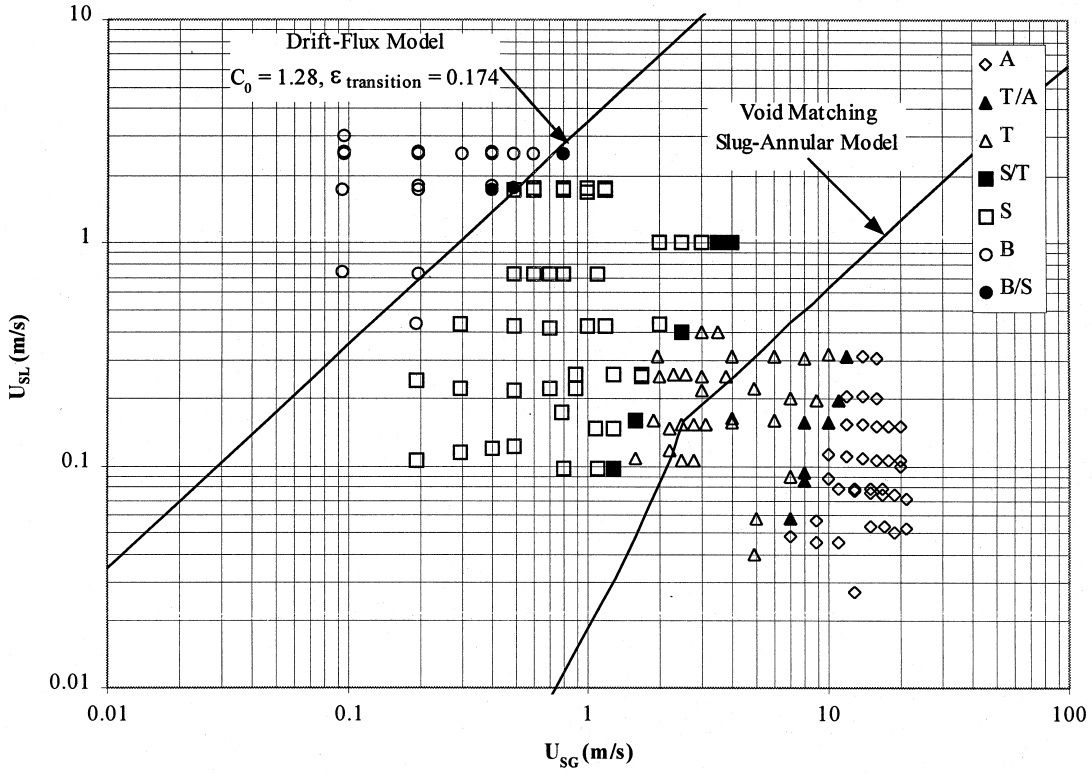

Fig. 15. Superficial velocity flow regime map comparing the drift–flux model (Bousman et al., 1996) and the void matching slug annular model (Bousman, 1995) to the current date set: A = annular, T/A = transitional/annular, T = transitional, S/T = slug/transitional, S = slug, B/S = bubbly/slug, B = bubbly.

number, defined as:

$$We = \frac{U^2 D\rho}{\sigma} = \frac{\text{inertial force}}{\text{surface tension}}, \tag{3}$$

represents the ratio between the two dominant forces. In Eq. (3), U is the phase velocity, ρ is the phase density, and σ is surface tension. Since the Weber number includes the phase velocity term, and in the absence of actual phase velocity measurements, the liquid and gas Weber numbers are calculated in terms of the superficial velocities, as follows:

$$We_{\mathrm{SL}} = \frac{U_{\mathrm{SL}}^2 D\rho_{\mathrm{L}}}{\sigma_{\mathrm{L}}} \tag{4}$$

and

$$We_{\mathrm{SG}} = \frac{U_{\mathrm{SG}}^2 D\rho_G}{\sigma_{\mathrm{L}}} \tag{5}$$

In Eqs. (4) and (5), σ_{L} is the liquid–air surface tension.

Zhao and Rezkallah (1993) suggested that bubbly and slug flows are surface tension dominated flows, and will thus occur at low We_{SG}. Annular flow is inertia dominated so it will occur at large values of We_{SG}. In transitional flow, inertia and surface tension forces are comparable, and hence they occupy the region between annular and slug flow. They also predicted that the transitional flow regime begins at a value of We_{SG} equal to about 1, and the onset to annular flow occurs at a We_{SG} equal to approximately 20. Later studies by Rezkallah and Zhao (1995) and Rezkallah (1996) revised this map and gave each transition line an upwards slope of approximately 1:4.

Fig. 16 is the Weber number based flow regime map including the present data set. The line proposed by Rezkallah (1996) separating slug and transitional flow fits the new data very well, while the one separating transitional and annular flow seems to slightly over-predict the transition. Those lines, however have the correct slope, as predicted by Rezkallah and Zhao (1995). The over-prediction is likely due to the difficult and highly subjective video flow regime identification method used to determine the flow regimes upon which the transition line was based. It is the author's experience that determining whether a flow is fully annular or transitional using only video images is a very difficult task. This study presents a mainly objective method of determining flow regimes, and hence less reliance on the subjectivity of 2-D video observations.

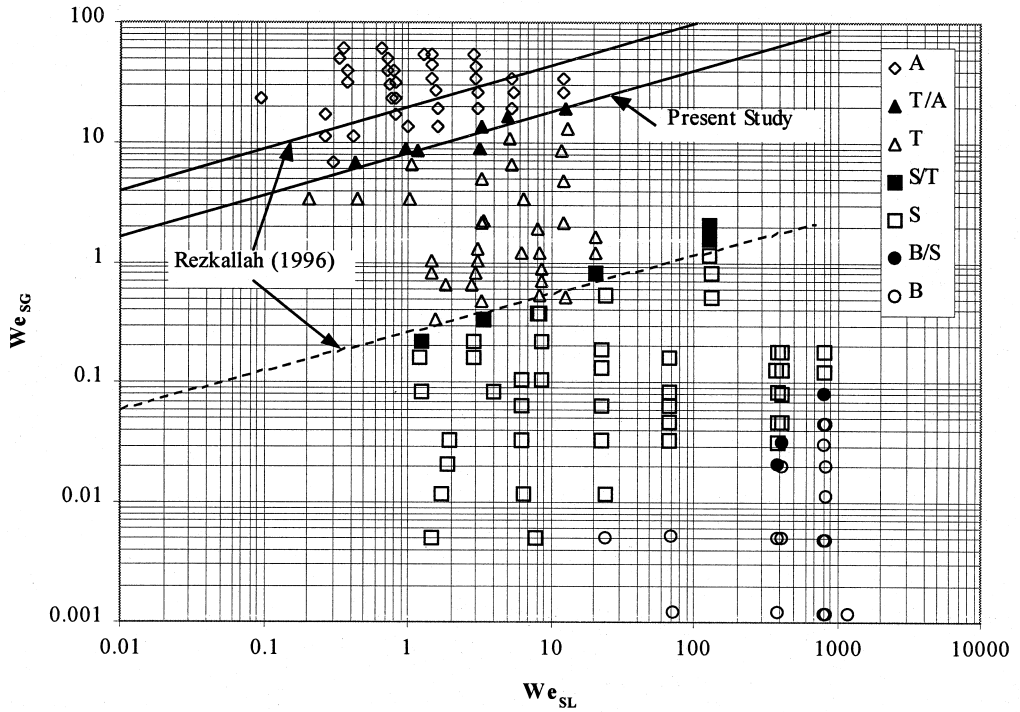

Fig. 16. Weber number flow regime map comparing the current data set to the Weber number model (Rezkallah, 1996): A = annular, T/A = transitional/annular, T = transitional, S/T = slug/transitional, S = slug, B/S = bubbly/slug, B = bubbly.

6. Conclusions

This paper presented an objective method of flow regime identification for microgravity two-phase flows in a 9.525 mm tube. This method uses PDF analysis based on the signal from a capacitance type void fraction sensor. The following set of criteria were developed for identifying each flow regime:

Bubbly flow: a single peak in the void fraction PDF at a low void fraction, typically less than 0.20.

Slug flow: a double peaked PDF with one peak at a high void fraction and one at a low fraction. Some slug flows at low liquid velocities may show two peaks very close together.

Transitional flow: a single peak in the PDF at a high void fraction, with a tail extending down to void fractions less than 0.45.

Annular flow: a single sharp peak in the PDF at a high void fraction, typically between 0.80 and 0.90, with a short tail extending to void fractions no less than 0.50.

The transitions between the flow regimes are characterized by the following criteria:

Bubbly-to-slug: characterized by the onset of a second peak in the bubbly flow PDF, but two distinct peaks can not be clearly identified.

Slug-to-transitional: characterized by the near disappearance of the lower peak in the slug flow PDF.

Transitional-to-annular: characterized by the tail of the single peak in the PDF ending at a void fraction between 0.45 and 0.50.

With these criteria, the main flow regimes and the transitions between them can be easily, and for the most part, objectively identified from the void fraction PDF alone without the aid of flow images.

Three microgravity flow regime transition models were examined using the new data set and the flow regime identification criteria. It was found that while the drift–flux model predicted well the bubbly-to-slug transition, it was very dependant on the value of the transition void fraction chosen, and also on the value of C_0. The void matching slug-to-annular transition model suggested by Bousman (1995) gives a line which falls within the broad range of flow rates covered by the transitional flow regime, but it does not delineate slug flow from transitional flow, or transitional flow from annular flow. However, the Weber number model is quite successful in predicting the boundaries between slug and transitional flow, and between transitional and annular flow.

Acknowledgements

The authors acknowledge the financial support received for this project from the College of Engineering, University of Saskatchewan, NSERC, and the provision of the DC-9 flight by the Canadian Space Agency.

References

Bousman, S., 1995. Studies of two-phase gas–liquid flow in microgravity. PhD thesis, University of Houston, Texas.

Bousman, W.S., McQuillen, J.B., Witte, L.C., 1996. Gas–liquid flow patterns in microgravity: effects of tube diameter, liquid viscosity and surface tension. Int. J. Multiphase Flow 22, 1035–1053.

Colin, C., Fabre, J., 1995. Gas–liquid pipe flow under microgravity conditions: influence of tube diameter on flow patterns and pressure drops. Adv. Space Res. 16, 137–142.

Costigan, G., Whalley, P.B., 1997. Slug flow regime identification from dynamic void fraction measurements in vertical air–water flows. Int. J. Multiphase Flow 23, 263–282.

Dukler, A.E., Fabre, J.A., McQuillen, J.B., Vernon, R., 1988. Gas–liquid flow at microgravity conditions: flow patterns and their transitions. Int. J. Multiphase Flow 14, 389–400.

Elkow, K.J., 1995. Void fraction measurement and analysis at normal gravity and microgravity conditions. M.Sc. thesis, University of Saskatchewan, Saskatoon, Canada.

Elkow, K.J., Rezkallah, K.S., 1997. Statistical analysis of void fluctuations in gas–liquid flows under 1-G and μ-G conditions using a capacitance sensor. Int. J. Multiphase Flow 23, 831–844.

Jones, O.C., Zuber, N., 1975. The interrelation between void fraction fluctuations and flow patterns in two-phase flow. Int. J. Multiphase Flow 2, 273–306.

Lowe, Devin C., 1997. A study on flow regime identification in microgravity gas–liquid flows using a capacitance sensor. M.Sc. thesis, University of Saskatchewan, Saskatoon, Canada.

Rezkallah, K.S., 1996. Weber number based flow-pattern maps for liquid–gas flows at microgravity. Int. J. Multiphase Flow 22, 1265–1270.

Rezkallah, K.S., de Jong, P., 1998. A study of annular two-phase flow characteristics under microgravity conditions. In: Proc. of the First Pan-Pacific Workshop on Microgravity. Japan Society Microgravity Applications, Tokyo.

Rezkallah, K.S., Zhao, L., 1995. Flow pattern map for two-phase liquid–gas flows under reduced gravity conditions. J. of Advances in Space Research 16, 133–136.

Song, C.H., No, H.C., Chung, M.K., 1995. Investigation of bubble flow developments and its transition based on the instability of void fraction waves. Int. J. Multiphase Flow 21, 381–404.

Zhao, L., Rezkallah, K.S., 1993. Gas–liquid flow patterns at microgravity conditions. Int. J. Multiphase Flow 19, 751–763.

Zuber, N., Findlay, J.A., 1965. Average volumetric concentration in two-phase flow systems. Journal of Heat Transfer, Trans. ASME, Series C 87, 453–468.